Noninvasive Prediction of High-Grade Prostate Cancer via Biparametric MRI Radiomics

Lixin Gong, MS,[1,2†] Min Xu, MS,[3†] Mengjie Fang, MS,[2,4] Jian Zou, PhD,[5] Shudong Yang, MD,[6] Xinyi Yu, MS,[3] Dandan Xu, MS,[3] Lijuan Zhou, MS,[3] Hailin Li, MS,[2] Bingxi He, MS,[2,4] Yan Wang, MS,[3] Xiangming Fang, MD,[3*] Di Dong, PhD,[2,4*] and Jie Tian, PhD[1,2,7*]

Background: Gleason score (GS) is a histologic prognostic factor and the basis of treatment decision-making for prostate cancer (PCa). Treatment regimens between lower-grade (GS ≤7) and high-grade (GS >7) PCa differ largely and have great effects on cancer progression.

Purpose: To investigate the use of different sequences in biparametric MRI (bpMRI) of the prostate gland for noninvasively distinguishing high-grade PCa.

Study Type: Retrospective.

Population: In all, 489 patients (training cohort: N = 326; test cohort: N = 163) with PCa between June 2008 and January 2018.

Field Strength/Sequence: 3.0T, pelvic phased-array coils, bpMRI including T_2-weighted imaging (T_2WI) and diffusion-weighted imaging (DWI); apparent diffusion coefficient map extracted from DWI.

Assessment: The whole prostate gland was delineated. Radiomic features were extracted and selected using the Kruskal–Wallis test, the minimum redundancy-maximum relevance, and the sequential backward elimination algorithm. Two single-sequence radiomic (T_2WI, DWI) and two combined (T_2WI-DWI, T_2WI-DWI-Clinic) models were respectively constructed and validated via logistic regression.

Statistical Tests: The Kruskal–Wallis test and chi-squared test were utilized to evaluate the differences among variable groups. $P < 0.05$ determined statistical significance. The area under the receiver operating characteristic curve (AUC), specificity, sensitivity, and accuracy were used to evaluate model performance. The Delong test was conducted to compare the differences between the AUCs of all models.

Result: All radiomic models showed significant ($P < 0.001$) predictive performances. Between the single-sequence radiomic models, the DWI model achieved the most encouraging results, with AUCs of 0.801 and 0.787 in the training and test cohorts, respectively. For the combined models, the T_2WI-DWI models acquired an AUC of 0.788, which was almost the same with DWI in the test cohort, and no significant difference was found between them (training cohort: $P = 0.199$; test cohort: $P = 0.924$).

Data Conclusion: Radiomics based on bpMRI can noninvasively identify high-grade PCa before the operation, which is helpful for individualized diagnosis of PCa.

Level of Evidence: 4

Technical Efficacy Stage: 2

PROSTATE CANCER (PCa) ranks second in fatal cancer causes for men in 2019 as the most commonly diagnosed male cancer in the United States.[1,2] Early diagnosis and treatment can effectively improve survival rates among PCa patients.[3]

According to the treatment guidelines recommended by the National Comprehensive Cancer Network,[4] the Gleason score (GS) is one of the most important factors in the diagnosis of PCa. Patients can be categorized into GS ≤7 (lower-grade PCa) and GS >7 (high-grade PCa) with an incidence of ~15% in PCa patients.[5,6] A study has shown that the 5-year recurrence-free progression probabilities for lower-grade PCa (63–96%) and high-grade PCa (26–48%) have great differences.[7] Lower-grade PCa patients may benefit from relatively conservative treatment strategies or short-time neoadjuvant antiandrogen therapy (ADT) for 4–6 months, while high-grade PCa patients are suggested a longer ADT with 2–3 years that may improve the prognosis and reduce mortality.[4,8,9] However, GS can only be determined via needle biopsy or resection.[10–12] Therefore, accurate noninvasive determination of high-grade PCa at the initial diagnosis or before surgery is very important for treatment decision-making and the prognosis of patients.

Although previous studies have highlighted the potential role of magnetic resonance imaging (MRI) for predicting PCa (including high-grade PCa),[13–16] there is no clear consensus on a robust biomarker of images in assessing its aggressiveness. Furthermore, radiologists' diagnoses of PCa are relatively subjective, relying on clinical experience.

Recently, radiomic analysis that enables extracting huge amounts of quantitative features from images has been utilized to aid in clinical decision-making in many cancers.[17,18] Also, radiomic approaches that aim to identify the presence of disease, non-invasively discriminate grade or stage, and stratify disease risk based on MRI have been proposed.[19,20] Several studies have demonstrated that texture features from the tumor region on MRI could distinguish GS, identify PCa, and determine aggressiveness.[15,16,21] However, few previous studies evaluated the capability of differences of different sequences of biparametric MRI (bpMRI).

In this study we aimed to investigate the value of bpMRI radiomics in the prediction of high-grade PCa.

Materials and Methods

Patients and MRI Data Acquisition

We retrospectively enrolled PCa patients treated at our hospital from June 2008 to January 2018, with GS determined by pathology. The requirement for informed consent was waived by the Ethics Committee of the hospital. The study design is shown in Fig. 1.

3.0T MR scanners at a single institution (Magnetom Verio, Siemens Healthcare, Erlangen, Germany) using pelvic phased-array coils were applied to scan all the patients. For each standard prostatic MRI examination conducted, T_2-weighted imaging (T_2WI) and diffusion-weighted imaging (DWI) were included. The apparent diffusion coefficient (ADC) map was also calculated from the DWI. Table 1 shows the scanning parameters of bpMRI.

In our hospital, the scanning protocols were in strict accordance with the requirements of the latest guidelines, and the b-values were scanned from b-0 to high b value series step-by-step (2008–2015 b-value: 0, 50, 100, 150, 200, 400, 600, 800 s/mm^2; after 2015 b-value: 0, 50, 100, 150, 200, 600, 800, 1600 s/mm^2). Therefore, in our study we used a b-value of 800 s/mm^2, since most of the patients have this b-value DWI image.

The inclusion criteria were as follows: 1) patients diagnosed with PCa by pathology; 2) patients who underwent MRI examination before pathological examination, including T_2WI and DWI; 3) the interval between MRI capture and pathological examination of less than 6 weeks; 4) pathological examination with a specific GS
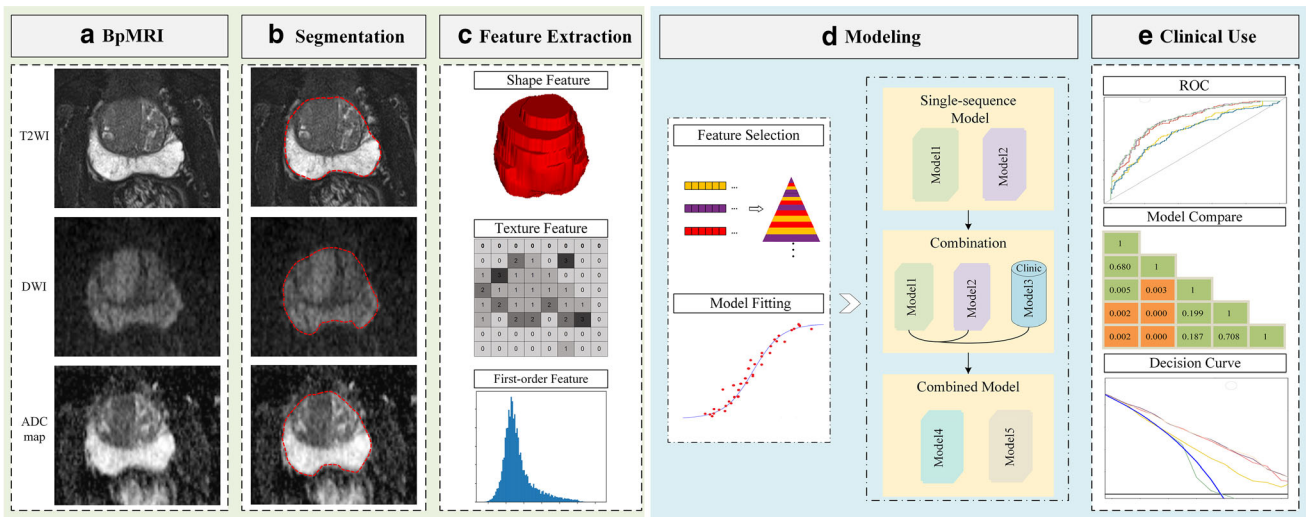
FIGURE 1: The pipeline of MRI radiomics analysis for predicting high-grade PCa. (a) Biparametric MRI findings for PCa. (b) Segmentation by radiologists. (c) Extraction of radiomic features. (d) Selection of features, the development of single-sequence and combined models. (e) Evaluation of the models using AUC, Delong test, and decision curves. GS = Gleason score; PCa = prostate cancer; MRI = magnetic resonance imaging; AUC = the area under the receiver operating characteristic curve.

TABLE 1. Scanning Parameters of Each MRI Sequence

Parameter	Axial T$_2$W	Axial DWI
TR (msec)	4000	3200
TE (msec)	100	84
Slice thickness (mm)	3	3
Flip angle (°)	150	90
Intersection gap (mm)	3	3
Pixel spacing	0.75/0.75	1.95/1.95
Matrix	320 × 259	192 × 192
FOV (mm)	216 × 240	250 × 250

DWI = diffusion weighted imaging; T$_2$W = T$_2$ weighted; TR = repetition time; TE = echo time; FOV = field of view.

score and meeting the following conditions: for patients with a systemic puncture with 12 + X needle biopsy, GS scores of specimens from different cancer areas were the same; for patients who underwent radical prostatectomy, GS scores of different cancer areas in postoperative pathology were the same.

The exclusion criteria were: 1) incomplete clinical data; 2) poor image quality that was unable to outline the prostate.

Between June 2008 and January 2018, there were 602 candidate patients satisfied the inclusion criteria and 113 patients were excluded, leaving a total of 489 eligible patients (72.79 ± 7.20 years old) including 275 patients with a systematic puncture and 214 patients who underwent radical prostatectomy. Among them, 238 belonged to the lower-grade PCa group and 251 to the high-grade one.

In this study two-thirds of the total samples were randomly selected as the training cohort (N = 326), while the remaining patients were included in the test cohort (N = 163).

Clinical Characteristics
In this study prostate-specific antigen (PSA) levels, PSA density (PSAD), and age were analyzed as potential clinical factors (Supplementary 1). Univariate analyses were performed to explore the significances of these clinical characteristics in the training and test cohorts.

The clinically significant characteristics were used to construct a clinical model via logistic regression (LR) for high-grade PCa prediction. In this process, the area under the receiver operating characteristic (ROC) curve (AUC), specificity (SP), sensitivity (SE), and accuracy (ACC) were calculated to evaluate the performance of the model.

Region of Interest Masking
ITK-SNAP v. 3.4.0 (www.itksnap.org) was utilized for 3D manual segmentation in bpMRI including T$_2$WI, DWI, and ADC map.

Without knowing the clinical information and pathological results of patients, a radiologist with 5 years of experience (reader 1) in reading MRI segmented the whole prostate gland layer-by-layer as the region of interest (ROI) on T$_2$WI, DWI, and the ADC map, separately. The prostate was roughly outlined according to the Prostate Imaging Reporting and Data System (PI-RADS) v2,[22] and the clinically

peripheral zone and transitional zone were mainly used. Anatomical landmarks such as the urethra, ejaculatory ducts, and prostatic capsule were used to determine the ROI, and the surrounding fat, muscle tissue, large blood vessels, and veins were excluded.

To assess the accuracy of the manual segmentations, 60 samples were randomly selected from the training cohort to be resegmented by reader 1 and another radiologist (reader 2) with over 10 years of experience in evaluating prostate MRIs after 3 months. Further details can be found in the Supplementary 2.

Radiomic Feature Extraction and Selection
Radiomic features were extracted using the package of Pyradiomics in Python (v. 3.6; https://www.python.org/).[23] Three groups of features including first-order statistical, shape, and textural features were extracted from the bpMRI of the ROI.

In this study the extracted radiomic features were selected using the Kruskal–Wallis test and the minimum redundancy-maximum relevance (mRMR). The parameter within the mRMR was set using a grid search with 10-fold cross-validation. LR analysis with the sequential backward elimination (SBE) algorithm was then adopted to choose the key features (see Supplementary 3). The preprocess for data is detailed in the Supplementary 4.

Single-Sequence Radiomic Model Construction and Validation
Employing the selected key features, two single-sequence radiomic models were respectively constructed via LR analyses in the training cohort, including a T$_2$WI model and a DWI model. Specifically, the model T$_2$WI was constructed by the key features of T$_2$WI of bpMRI; the model DWI was constructed by the radiomic scores (Supplementary 5) of the DWI images and ADC map, since the ADC map was calculated from DWI images and they basically evaluated the same thing. The models were then evaluated in the test cohort via AUC, SP, SE, and ACC.

Combined Model Construction and Validation
To investigate the predictive power of the combined sequences of MRI, a combined radiomic model, T$_2$WI-DWI, was then constructed via LR analysis based on the combinations of the single-sequence radiomic models T$_2$WI and DWI. Note that the construction and evaluation of T$_2$WI-DWI utilized the same method as the single-sequence radiomic models.

Since the clinical information is routinely available, T$_2$WI-DWI-Clinic models, the combination of radiomic models and clinically significant characteristics, were also constructed and validated utilizing the same method as the single-sequence and combined radiomic models.

To compare the models we constructed, the Delong test was performed on the AUCs of different models, and the net reclassification index (NRI) was also calculated to determine the incremental predictive value of a sequence when necessary.

Statistical Analyses
The Kruskal–Wallis test was utilized to evaluate the differences among the discrete variable groups, while a chi-squared test was applied to examine the differences between continuously variable groups. Two-sided statistical tests were conducted and the statistical significance was determined when $P < 0.05$. The Delong test was

conducted to quantitatively compare the differences between the AUCs of the two models. Decision curve analysis (DCA), aiming to identify the maximum net benefit, was utilized to analyze the model's benefit to the patients. R software for Windows (v. 3.5.1; https://www.r-project.org) was applied for all statistical analyses.

Results

Clinical Characteristics and Clinical Model Performance

Patient characteristics are summarized in Table 2. Both PSAD and PSA showed significant differences between high-grade and lower-grade PCa ($P < 0.001$). However, age was not identified as a significant factor ($P = 0.203$).

The performance and ROC curves of the clinical model are shown in Table 3 and Fig. 2, which exhibited poor performances in both the training (AUC: 0.696, SP: 0.641, SE: 0.686, ACC: 0.663) and test (AUC: 0.723, SP: 0.655, SE: 0.684, ACC: 0.669) cohorts.

Feature Discovery and Selection

In total, we extracted 1345 features from T_2WI, DWI, and the ADC map of the ROI: 265 first-order statistical features, 13 morphological features, and 1067 texture features.

After the feature selection step, 3, 5, and 8 key features were finally reserved in T_2WI, DWI, and the ADC map, respectively, which are shown in Supporting Table A.2.

We found that most of the key features were textural features, such as large area low gray level emphasis, zone variance, and cluster prominence, which might reflect the heterogeneity and invasiveness of the tumor. In addition, we found that the first-order statistic features, such as the median gray level intensity, 10th percentile, 90th percentile, interquartile range, kurtosis, etc., also showed significant contributions in predicting high-

grade PCa. The first-order statistic features described the voxel intensities' distribution, and our results may demonstrate that the intensity of the signal in MRI is correlated with the grade of PCa.

Single-Sequence Radiomic Model Construction and Validation

Relying on the key feature sets, two single-sequence radiomic models (T_2WI and DWI) were constructed using LR, and the involved radiomic scores of bpMRI are shown in Supplementary 5 and their violin plots are illustrated in Fig. A1. Both single-sequence radiomic models showed significant effectiveness in high-grade PCa prediction ($P < 0.001$). The quantitative metrics and the ROC curves of the single-sequence models are shown in Table 3 and Fig. 2, respectively.

Between the single-sequence radiomic models, the model DWI achieved a relatively satisfactory result, with AUC of 0.801, SP of 0.731, SE of 0.755, and ACC of 0.742 in the training cohort, while AUC of 0.787, SP of 0.726, SE of 0.671, and ACC of 0.699 in the test cohort. In contrast, the T_2WI had a worse performance in both the training and test cohorts (training cohort: AUC = 0.712, SP = 0.701, SE = 0.642, ACC = 0.672; test cohort: AUC = 0.645, SP = 0.691, SE = 0.544, ACC = 0.620), which is also lower than the clinical model in the test cohort (AUC = 0.723, SP = 0.655, SE = 0.684, ACC = 0.669).

Combined Model Construction and Validation

The combined radiomic model T_2WI-DWI showed significant effectiveness in high-grade PCa prediction ($P < 0.001$). In the training cohort, it got a little better performance (AUC = 0.811, SP = 0.713, SE = 0.786, ACC = 0.749) than DWI. In the test cohort, it (AUC = 0.788) acquired roughly the same AUC with DWI (AUC = 0.787). Specifically, the

TABLE 2. Clinical Characteristics of Patients in the Training and Test Cohorts

Clinical characteristics	Training cohort		Univariate analysis P value*	Test cohort		Univariate analysis P value*
	LOW PCa	HIGH PCa		LOW PCa	HIGH PCa	
No. of patients	167	159		84	79	
Age, years (Mean ± SD)	72.15 ± 6.95	72.76 ± 6.80	0.57 (Z = 0.32)	72.51 ± 7.39	74.49 ± 8.10	0.20 (Z = 1.62)
PSA			1.71×10^{-9} (Z = 36.28)			8.62×10^{-7} (Z = 24.21)
<10 ng/mL	44	16		20	7	
≥10 ng/mL	123	143		64	72	
PSAD			1.53×10^{-9} (Z = 36.49)			2.66×10^{-6} (Z = 22.05)
<0.45 ng/mL^2	62	23		34	15	
≥0.45 ng/mL^2	105	136		50	64	

LOW PCa = lower-grade prostate cancer; HIGH PCa = high-grade prostate cancer; Z = the statistics; PSA = prostate-specific antigen; PSAD = PSA density; SD = standard deviation; *Kruskal–Wallis tests were used to assess the differences among the discrete variable groups, while chi-squared test was used to test the differences between continuously variable groups.

TABLE 3. Performance of Clinical and Radiomic Models

Model		AUC	SP	SE	ACC
Training cohort					
Clinical model		0.696 (0.639, 0.753)	0.641	0.686	0.663
Single-Sequence radiomic model	T$_2$WI	0.712 (0.657, 0.768)	0.701	0.642	0.672
	DWI	0.801 (0.754, 0.848)	0.731	0.755	0.742
Combined model	T$_2$WI-DWI	0.811 (0.766, 0.857)	0.713	0.786	0.749
	T$_2$WI-DWI-Clinic	0.813 (0.767, 0.859)	0.784	0.723	0.755
Test cohort					
Clinical model		0.723 (0.645, 0.802)	0.655	0.684	0.669
Single-Sequence radiomic model	T$_2$WI	0.645 (0.560, 0.730)	0.691	0.544	0.620
	DWI	0.787 (0.718, 0.857)	0.726	0.671	0.699
Combined model	T$_2$WI-DWI	0.788 (0.719, 0.858)	0.738	0.658	0.699
	T$_2$WI-DWI-Clinic	0.780 (0.710, 0.851)	0.762	0.595	0.681

Clinic = the clinical model; T$_2$WI = the model of T$_2$ weighted imaging; DWI = the model of diffusion weighted imaging and the apparent diffusion coefficient map; AUC = the area under the receiver operating characteristic curve; SP = specificity; SE = sensitivity; ACC = accuracy.

SE of the latter was 0.671, which was slightly higher than the former (SE = 0.658) in the test cohort (Table 3 and Fig. 2). The NRI analysis revealed that there was no significant improvement (NRI: −0.001; P = 0.492) in the addition of the T$_2$WI sequence into the DWI model.

T$_2$WI-DWI-Clinic had a lower AUC of 0.780 compared to T$_2$WI-DWI (AUC = 0.788) in the test cohort (Table 3). To evaluate the additional contribution of clinical characteristics to the combined radiomic model, we further conducted a multivariable analyses for T$_2$WI-DWI-Clinic, and found that they were not significant (PSA: P = 0.251, PSAD: P = 0.519).

Comparison of Models

Figure 3 details the comparison results on the AUCs of different models using the Delong test. There were no significant performance differences between the single-sequence models and the
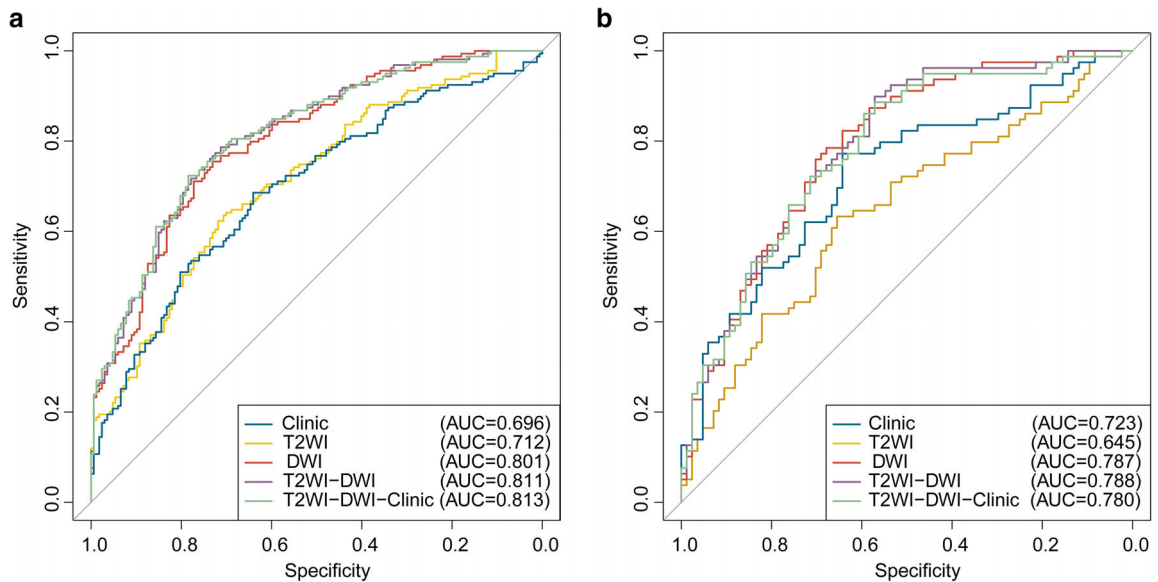
FIGURE 2: Comparison of single-sequence radiomic and combined model. (a) ROCs in the training cohort. (b) ROCs in the test cohort. ROCs = receiver operating characteristic curves.
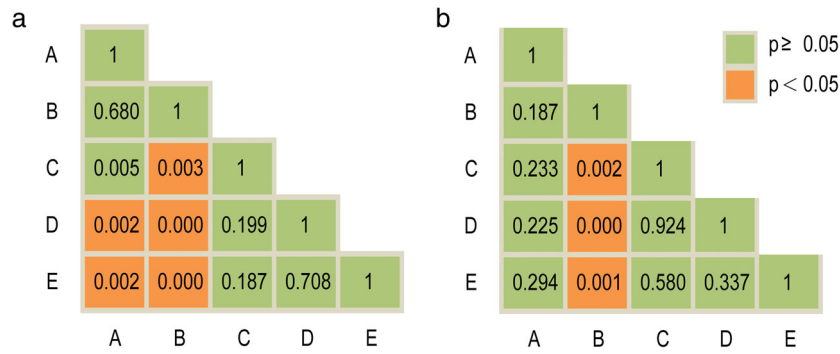
FIGURE 3: Delong test for AUCs of two models. (a): Delong test for AUCs of two models in the training cohort; (b): Delong test for AUCs of two models in the test cohort. A = the clinical model; B = the model of T_2WI; C = the model of DWI; D = the combined model of T_2WI and DWI; E = the combined model of T_2WI, DWI and clinically significant characteristics; AUC = the area under the receiver operating characteristic curve.

clinical model in the training and test cohorts (training cohort: T_2WI: $P = 0.680$, DWI: $P = 0.005$; test cohort: T_2WI: $P = 0.187$, DWI: $P = 0.233$). Both the combined model T_2WI-DWI and T_2WI-DWI-Clinic had significant advantages compared to the single-sequence radiomic model T_2WI in the training and test cohorts ($P < 0.05$). On the contrary, Both the combined model T_2WI-DWI and T_2WI-DWI-Clinic were not significantly different from the single-sequence radiomic model DWI in the training and test cohorts (training cohort: T_2WI-DWI: $P = 0.199$, T_2WI-DWI-Clinic: $P = 0.187$; test cohort: T_2WI-DWI: $P = 0.924$, T_2WI-DWI-Clinic: $P = 0.580$). Also, they showed significant improvement to the clinical model in the training cohort ($P < 0.05$), but not in the test cohort (T_2WI-DWI: $P = 0.225$, T_2WI-DWI-Clinic: $P = 0.294$). There were no significant improvements in the addition of the clinical characteristics to the T_2WI-DWI (training cohort: $P = 0.708$, test cohort: $P = 0.337$).

FIGURE 4: Decision curve analyses of radiomic models and clinical model.
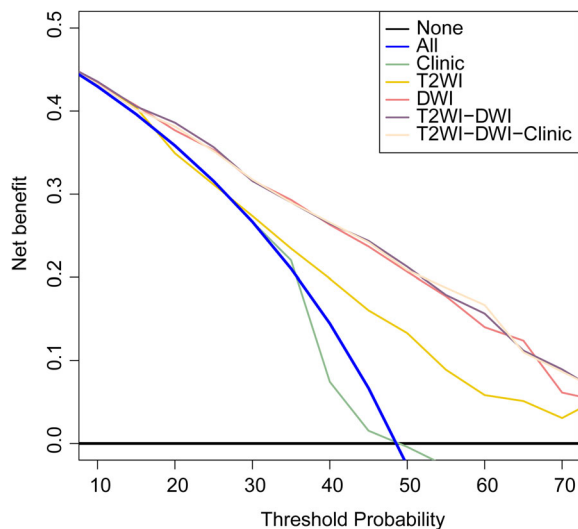
Clinical Use

The DCA results for the combined models and clinical models are shown in Fig. 4, According to which, the single-sequence model DWI and the combined models displayed higher benefit to patients than a treat-all-as-high-grade scheme or treat-none-as-high-grade scheme, while the T_2WI and clinical models exhibited poor benefit.

Discussion

In this retrospective study, we conducted a biparametric radiomic analysis to identify high-grade PCa patients. The single-sequence and combined models based on the ROI of the whole prostate gland showed good predictive performance.

Our findings demonstrated that the single-sequence model DWI had the best prediction performance for high-grade PCa. By contrast, the addition of T_2WI had relatively little effect on predictive performance. The reason for this may be that the DWI and ADC map indirectly reflect the change of microstructure by detecting the degree of limited diffusion of water molecules in human tissues and organs,[24] while the T_2 sequence was usually used to demonstrate the anatomical structure of the prostate gland. However, when adding clinical information to the combined radiomic model, no performance improvements were found; the reason may be that the clinical information was not significant in multivariable analysis.

Many previous studies have investigated textural analyses in GS staging using MRI. Wibmer et al[25] investigated the roles of the Haralick texture from MRI in differentiating GS ≤7 vs. GS >7 and revealed the effectiveness of the ADC map for GS staging. Vignati et al[26] and Chaddad et al[27] highlighted the value of texture features in predicting GS. Turkbey et al[28] and Donati et al[29] proved that the ADC map was useful in predicting the aggressiveness of PCa. In good agreement with the previous research, our study further supported the role of textural features and DWI with ADC map in predicting high-grade GS. Additionally, we also found

the first-order statistical features, such as the 10th percentile, 90th percentile, interquartile range, etc., were worthwhile in predicting high-grade PCa.

Besides the textural analyses, previous studies also focused on the combination of different MRI sequences. Shimofusa et al[30] conducted a retrospective study based on the performance of three readers and reported that T_2W with DWI had more predictive ability in detecting PCa than T_2W alone, which matches well with our findings. Huadong et al[31] Evaluated the capabilities of T_2WI, DWI, and ADC map by two radiologists, finding that the DWI with ADC map performed better than T_2WI in detecting PCa, which is consistent with our results.

Furthermore, previous studies mainly analyzed the features of tumor, involving sophisticated tumor segmentation. In 2013, Tanaka et al[32] found that the volume of the whole prostate gland showed a significantly greater predictive power than serum PSA for predicting PCa. In 2015, Peng et al[33] reported that the prostate volumes had similar predictive performance compared to central-gland volumes from T_2WI for the diagnosis of PCa. Inspired by their studies, we performed an analysis on the whole gland, which contained both information on the tumor and its surroundings.[34] The gland segmentation can avoid the mismatching phenomenon and inaccurate segmentation caused by image deformation between T_2WI and DWI.[35] Meanwhile, the gland segmentation is easier to achieve than the segmentation of tumor zone, which may also support the application of automatic or semiautomatic segmentation.[36]

Compared to the DWI and the combined models, the clinical model was less accurate in both the training and test cohorts, revealing the limited predictability of the present clinical predictors for PCa. Previous relevant studies[37,38] had already proven that a certain correlation exists between the referred clinical factors and PCa grading. Consistent with previous researches, our study indicated that PSA, PSAD were relevant to GS. However, the nonsignificant results of them in multivariable analyses and the few benefits of adding them to the radiomic models revealed their limited predictive performance compared to the radiomic models. In contrast to the earlier findings,[37] no significant correlation between age and GS was found in our study. The inconsistency may be due to the limited number of patients, and a further test of our models should be performed on a large-scale cohort.

Limitations

First, this was a single-center study; the findings need to be further validated in larger populations. Second, the PI-RADS scoring system is an important MRI indicator of PCa in the clinic, but we failed to incorporate the PI-RADS score in our study. The reason is that the MRI sequences of some patients do not meet the latest PI-RADS v2 grading guidelines. Third,

this study used a b-value of 800 s/mm^2 for DWI. Other b-value series should be considered in future studies.

Conclusion

Our study demonstrates that radiomics-based models incorporating high-dimensional bpMRI features have the potential to identify high-grade PCa patients.

Conflicts of Interest

There are no conflicts of interest to declare.

References

1. Siegel RL, Miller KD, Jemal A. Cancer statistics, 2019. CA Cancer J Clin 2019;69(1):7-34.

2. Negoita S, Feuer EJ, Mariotto A, et al. Annual report to the nation on the status of cancer, part II: Recent changes in prostate cancer trends and disease characteristics. Cancer 2018;124(13):2801-2814.

3. Fedewa SA, Ward EM, Brawley O, Jemal A. Recent patterns of prostate-specific antigen testing for prostate cancer screening in the United States. JAMA Intern Med 2017;177(7):1040-1042.

4. Carroll PH, Mohler JL. NCCN guidelines updates: Prostate cancer and prostate cancer early detection. J Natl Compr Cancer Network 2018;16 (5S):620-623.

5. Van Poppel H, Joniau S. An analysis of radical prostatectomy in advanced stage and high-grade prostate cancer. Eur Urol 2008;53(2): 253-259.

6. Siegel RL, Miller KD, Jemal A. Cancer statistics, 2018. CA Cancer J Clin 2018;68(1):7-30.

7. Epstein JI, Zelefsky MJ, Sjoberg DD, et al. A contemporary prostate cancer grading system: A validated alternative to the Gleason score. Eur Urol 2016;69(3):428-435.

8. Miyake H, Sakai I, Inoue T-A, Hara I, Fujisawa M. The limited significance of a longer duration of neoadjuvant hormonal therapy prior to radical prostatectomy for high-risk prostate cancer in Japanese men. Urol Int 2006;77(2):122-126.

9. Hassan O, Han M, Zhou A, et al. Incidence of extraprostatic extension at radical prostatectomy with pure Gleason score 3+ 3= 6 (grade group 1) cancer: Implications for whether Gleason score 6 prostate cancer should be renamed "not cancer" and for selection criteria for active surveillance. J Urol 2018;199(6):1482-1487.

10. Albers LF, Korving JC, van Elzakker EP, Roshani H. Osteomyelitis of the pubic symphysis after transrectal biopsies of the prostate. Urology 2018;121:29-32.

11. van der Leest M, Cornel E, Israel B, et al. Head-to-head comparison of transrectal ultrasound-guided prostate biopsy versus multiparametric prostate resonance imaging with subsequent magnetic resonance-guided biopsy in biopsy-naïve men with elevated prostate-specific antigen: A large prospective multicenter clinical study. Eur Urol 2019;75(4):570-578.

12. Borghesi M, Ahmed H, Nam R, et al. Complications after systematic, random, and image-guided prostate biopsy. Eur Urol 2017;71(3):353-365.

13. Sato C, Naganawa S, Nakamura T, et al. Differentiation of non-cancerous tissue and cancer lesions by apparent diffusion coefficient values in transition and peripheral zones of the prostate. J Magn Reson Imaging 2005;21(3):258-262.

14. Tanimoto A, Nakashima J, Kohno H, Shinmoto H, Kuribayashi S. Prostate cancer screening: The clinical value of diffusion-weighted imaging and dynamic MR imaging in combination with T2-weighted imaging. J Magn Reson Imaging 2007;25(1):146-152.

15. Fehr D, Veeraraghavan H, Wibmer A, et al. Automatic classification of prostate cancer Gleason scores from multiparametric magnetic resonance images. Proc Natl Acad Sci U S A 2015;112(46):6265-6273.

16. Nketiah G, Elschot M, Kim E, et al. T2-weighted MRI-derived textural features reflect prostate cancer aggressiveness: Preliminary results. Eur Radiol 2017;27(7):3050-3059.

17. Dong D, Tang L, Li Z-Y, et al. Development and validation of an individualized nomogram to identify occult peritoneal metastasis in patients with advanced gastric cancer. Ann Oncol 2019;30(3):431-438.

18. Lambin P, Rios-Velazquez E, Leijenaar R, et al. Radiomics: Extracting more information from medical images using advanced feature analysis. Eur J Cancer 2012;48(4):441-446.

19. Xu M, Fang M, Zou J, et al. Using biparametric MRI radiomics signature to differentiate between benign and malignant prostate lesions. Eur J Radiol 2019;114:38-44.

20. Dong D, Zhang F, Zhong L-Z, et al. Development and validation of a novel MR imaging predictor of response to induction chemotherapy in locoregionally advanced nasopharyngeal cancer: A randomized controlled trial substudy (NCT01245959). BMC Med 2019;17(1):190-200.

21. Sidhu HS, Benigno S, Ganeshan B, et al. Textural analysis of multiparametric MRI detects transition zone prostate cancer. Eur Radiol 2017;27(6):2348-2358.

22. Weinreb JC, Barentsz JO, Choyke PL, et al. PI-RADS prostate imaging–reporting and data system: 2015, version 2. Eur Urol 2016;69(1):16-40.

23. van Griethuysen JJM, Fedorov A, Parmar C, et al. Computational radiomics system to decode the radiographic phenotype. Cancer Res 2017;77(21):e104-e107.

24. Yang K, Zhang XM, Yang L, Xu H, Peng J. Advanced imaging techniques in the therapeutic response of transarterial chemoembolization for hepatocellular carcinoma. World J Gastroenterol 2016;22(20):4835-4847.

25. Wibmer A, Hricak H, Gondo T, et al. Haralick texture analysis of prostate MRI: Utility for differentiating non-cancerous prostate from prostate cancer and differentiating prostate cancers with different Gleason scores. Eur Radiol 2015;25(10):2840-2850.

26. Vignati A, Mazzetti S, Giannini V, et al. Texture features on T2-weighted magnetic resonance imaging: New potential biomarkers for prostate cancer aggressiveness. Phys Med Biol 2015;60(7):2685-2701.

27. Chaddad A, Kucharczyk MJ, Niazi T. Multimodal radiomic features for the predicting Gleason score of prostate cancer. Cancer 2018;10(8):249-260.

28. Turkbey B, Shah VP, Pang Y, et al. Is apparent diffusion coefficient associated with clinical risk scores for prostate cancers that are visible on 3-T MR images? Radiology 2011;258(2):488-495.

29. Donati OF, Mazaheri Y, Afaq A, et al. Prostate cancer aggressiveness: Assessment with whole-lesion histogram analysis of the apparent diffusion coefficient. Radiology 2013;271(1):143-152.

30. Shimofusa R, Fujimoto H, Akamata H, et al. Diffusion-weighted imaging of prostate cancer. J Comput Assist Tomogr 2005;29(2):149-153.

31. Miao H, Fukatsu H, Ishigaki T. Prostate cancer detection with 3-T MRI: Comparison of diffusion-weighted and T2-weighted imaging. Eur J Radiol 2007;61(2):297-302.

32. Karademir I, Shen D, Peng Y, et al. Prostate volumes derived from MRI and volume-adjusted serum prostate-specific antigen: Correlation with Gleason score of prostate cancer. Am J Roentgenol 2013;201(5):1041-1048.

33. Peng Y, Shen D, Liao S, et al. MRI-based prostate volume-adjusted prostate-specific antigen in the diagnosis of prostate cancer. J Magn Reson Imaging 2015;42(6):1733-1739.

34. Delongchamps NB, Beuvon F, Mathieu JRR, et al. CXCR4 is highly expressed at the tumor front but not in the center of prostate cancers. World J Urol 2015;33(2):281-287.

35. Katelaris NC, Bolton DM, Weerakoon M, Toner L, Katelaris PM, Lawrentschuk N. Current role of multiparametric magnetic resonance imaging in the management of prostate cancer. Korean J Urol 2015;56(5):337-345.

36. Bulman JC, Toth R, Patel AD, et al. Automated computer-derived prostate volumes from MR imaging data: Comparison with radiologist-derived MR imaging and pathologic specimen volumes. Radiology 2012;262(1):144-151.

37. Isariyawongse BK, Sun L, Bañez LL, et al. Significant discrepancies between diagnostic and pathologic Gleason sums in prostate cancer: The predictive role of age and prostate-specific antigen. Urology 2008;72(4):882-886.

38. Vendrami CL, McCarthy RJ, Chatterjee A, et al. The utility of prostate specific antigen density, prostate health index and prostate health index density in predicting positive prostate biopsy outcome is dependent on the prostate biopsy Methods. Urology 2019;129:153-159.